Acta Astronautica 99 (2014) 215–230

Contents lists available at ScienceDirect

Acta Astronautica

journal homepage: www.elsevier.com/locate/actaastro

High-fidelity numerical simulation of complex dynamics of tethered spacecraft

Taeyoung Lee [a,*], Melvin Leok [b], N. Harris McClamroch [c]

[a] Mechanical and Aerospace Engineering, George Washington University, Washington, DC 20052, United States
[b] Mathematics, University of California at San Diego, La Jolla, CA 92093, United States
[c] Aerospace Engineering, University of Michigan, Ann Arbor, MI 48109, United States

ARTICLE INFO

Article history:
Received 25 January 2013
Received in revised form
7 February 2014
Accepted 21 February 2014
Available online 12 March 2014

Keywords:
Geometric numerical integrator
Tethered spacecraft
Numerical simulation

ABSTRACT

This paper presents an analytical model and a geometric numerical integrator for a tethered spacecraft model that is composed of two rigid bodies connected by an elastic tether. This high-fidelity model includes important dynamic characteristics of tethered spacecraft in orbit, namely the nonlinear coupling among tether deformations, rigid body rotational dynamics, a reeling mechanism, and orbital dynamics. A geometric numerical integrator, referred to as a Lie group variational integrator, is developed to numerically preserve the Hamiltonian structure of the presented model and its Lie group configuration manifold. This approach preserves the geometry of the configurations, and leads to accurate and efficient algorithms that have guaranteed accuracy properties that make them suitable for many dynamic simulations, especially over long simulation times. These analytical and computational models provide a reliable benchmark for testing the validity and applicability of the many simplified models in the existing literature, which have hitherto been used without careful verification that the simplifying assumptions employed are valid in physically realistic parameter regimes. We present numerical simulations which illustrate the important qualitative differences in the tethered spacecraft dynamics when the high-fidelity model is employed, as compared to models with additional simplifying assumptions.

1. Introduction

Tethered spacecraft are composed of multiple satellites in orbit, that are connected by a thin, long cable. Numerous innovative space missions have been envisaged, such as propulsion by momentum exchange, extracting energy from the Earth's magnetic field, satellite de-orbiting, or Mars exploration [1–3], and several actual missions, such as TSS, SEDS, or YES2 have been conducted by NASA and ESA [1,4].

The dynamics of tethered spacecraft involves nonlinear coupling effects between several dynamic modes evolving on multiple length and time scales. For example, a full scale tethered spacecraft may employ tethers with lengths up to a 100 km, while recently proposed nano-tethered spacecraft may employ short tethers of several meters in length. This is in stark contrast to the orbital radius of tethered spacecraft, which is several thousand kilometers. The natural frequency of the tether is much higher than the frequency of the rotational attitude dynamics or the orbital period of the spacecraft. The rotational dynamics of spacecraft is nontrivially coupled to the tension of the

* Corresponding author.
E-mail addresses: tylee@gwu.edu (T. Lee), mleok@math.ucsd.edu (M. Leok), nhm@umich.edu (N. Harris McClamroch).

http://dx.doi.org/10.1016/j.actaastro.2014.02.021
0094-5765/

tether, which is affected by the reeling mechanism and orbital maneuver. Therefore, it is important to accurately model tether dynamics, attitude dynamics of the spacecraft, reeling mechanisms, gravitational force and the interactions between them.

Several analytic and numerical models have been developed for tethered spacecraft. However, due to the complexities of tethered spacecraft, it is common practice to use simplified models. Two point masses connected by a rigid tether were considered in [5]. The dynamics of a massless, flexible tether was included in [6]. Transverse vibrations of two point masses connected by a flexible, but inextensible, tether were studied in [7]. The attitude dynamics of the payload satellite is considered in [8] in order to provide insights into the dynamics anomalies in the actual flight data of the OEDIPUS-A tethered rocket payload. However, this did not entail a fully coupled simulation, rather the paper addressed the response of the payload to prescribed disturbances in the tether tension, as opposed to explicitly including the dynamic coupling between the central satellite and the tether.

Vibration mode analysis is provided in [9–11], but a small vibrational amplitude assumption is imposed on the controlled tether [9]; the effect of an appendage extending at a prescribed rate is studied for a single spacecraft in [10]; and a linearized model of a spacecraft model connected to a fixed-length tether is studied in [11]. These simplified models allow for rigorous mathematical analysis, but they may fail to accurately predict the behavior of actual tethered spacecrafts, particularly since tethered spacecraft operations are typically based on weak nonlinear effects that act over a long time period. Recent numerical studies consider more sophisticated tethered spacecraft models including a varying tether length. But, in these advanced models, rigid body dynamics is ignored [12,13], and the reeling mechanism is neglected [12,14].

We have been motivated by these previous models to construct a high-fidelity mathematical and numerical model for elucidating the dynamics of tethered spacecraft where the tether is long relative to the dimensions of the spacecraft. This high-fidelity model can serve as a mathematical and computational testbed for exploring the extent to which nonlinear coupling between the various dynamic modes result in interesting and unforeseen phenomena that could serve as the basis for novel mission designs. While simplified models are desirable because of their computational efficiency and the ease with which they can be analyzed, as well as their applicability for real-time model predictive control in embedded applications, they typically have limited regimes of applicability in parameter space. Our high-fidelity model provides a reliable benchmark for determining the range of validity for the simplified models that have currently been studied, in an effort to determine which, if any, of the simplifying assumptions used in other models provide a valid simplified model in the parameter regimes for realistic tethered satellite missions.

For such applications, the primary deployment mechanism is through a reeling mechanism, and a careful model of the reeling mechanism is essential to resolving the coupled interactions among tether, reeling, and rotational dynamics. In particular, this allows us to resolve the elastic waves propagating along the tether, the dynamics of the reeling mechanism, rotational dynamics of the satellites, as well as the external forces arising from solar wind, atmospheric drag or electrodynamic effects. The long aspect ratio of the tether also means that there is effectively no resistance to bending and torsion in the tether, and the main effect is longitudinal elastic deformation along the tether. While bending can easily be incorporated by including an additional term in the potential energy, torsion will require us to consider a larger configuration space for the model. These assumptions and observations motivate the modeling choices that have been made in our model.

More precisely, the goal of this paper is to develop a high-fidelity analytical model and numerical simulations for tethered spacecraft. This is an extension of preliminary work that studies a string pendulum model with a reeling mechanism [15,16]. The first part of this paper provides a realistic and accurate analytical tethered spacecraft model including tether deformations, attitude dynamics of rigid bodies, and a reeling mechanism. We show that the governing equations of motion can be developed using Hamilton's principle.

The second part of this paper deals with a geometric numerical integrator for tethered spacecraft. Geometric numerical integration is concerned with developing numerical integrators that preserve the geometric features of a system, such as dynamical and geometric invariants, symmetries, and the structure of nonlinear configuration spaces [17]. Because these geometric invariants play an important role in the long-time qualitative and structural properties of a system, geometric structure-preserving integrators yield computational trajectories that more accurately reflect the qualitative and statistical properties of the system. These methods also exhibit more robust energy properties, and avoid the artificial numerical dissipation introduced by conventional integrators. A geometric numerical integrator, referred to as a Lie group variational integrator, has been developed for a Hamiltonian system on an arbitrary Lie group in [18]. The proposed method is competitive from the point of view of computational efficiency. Even though the method requires a nonlinear solve, this can be efficiently implemented using a fixed-point iteration, and the method only requires one force evaluation per time-step.

A tethered spacecraft is a Hamiltonian system, and its configuration manifold is expressed as the product of the Lie groups $\mathsf{SO}(3)$, $\mathsf{SE}(3)$, and the space of connected curve segments on $\mathbb{R}^3$. This paper develops a Lie group variational integrator for tethered spacecraft based on the results presented in [18]. The proposed geometric numerical integrator preserves symplecticity and momentum maps, and exhibits desirable energy conservation properties. It also respects the Lie group structure of the configuration manifold, and avoids the singularities and computational complexities associated with the use of local coordinates. It can be used to study non-local, large amplitude and deformation maneuvers of tethered spacecraft accurately over a long time period. This is in contrast to conventional approaches where small deformations are superimposed to a simplified, rigid tethered spacecraft

model and the important coupling effects between various dynamic modes are ignored.

The main contributions of this paper are summarized as follows: (i) a realistic mathematical model for tethered spacecraft that characterize the nonlinear coupling between the translation dynamics and the rotational dynamics of spacecraft, the translation and the deformation of the tether, and the reeling mechanism, (ii) unifying variational framework to develop equations of motion, (iii) high-fidelity numerical model to compute complex dynamics of tethered spacecraft accurately.

This paper is organized as follows. A tethered spacecraft model is described in Section 2. An analytical model and a Lie group variational integrator are developed in Sections 3 and 4, respectively, followed by numerical examples in Section 5.

2. Tethered spacecraft

We consider two rigid spacecrafts connected by an elastic tether. We assume that the rigid spacecrafts can freely translate and rotate in a three-dimensional space, and that the tether is extensible and flexible. The bending stiffness of the tether is neglected as the diameter of the tether is assumed to be negligible compared to its length. The tether is connected to a reeling drum in a base spacecraft, and the other end of the tether is connected to a sub-spacecraft. The point where the tether is attached to the spacecraft is displaced from the center of mass so that the rotational dynamics of the spacecraft is coupled to the tether deformations and displacements. This model is illustrated in Fig. 1.

We choose a global reference frame and two body-fixed frames. The global reference frame is located at the center of the Earth. The first body-fixed frame is located at the center of mass of the base spacecraft, and the second body-fixed frame is located at the end of the tether where the tether is attached to the sub-spacecraft. Since the tether is extensible, we need to distinguish between the arc length for the stretched deformed configuration and the arc length for the unstretched reference configuration. We now introduce some notations:

$m \in \mathbb{R}$ the mass of the base spacecraft, excluding the reeling mechanism

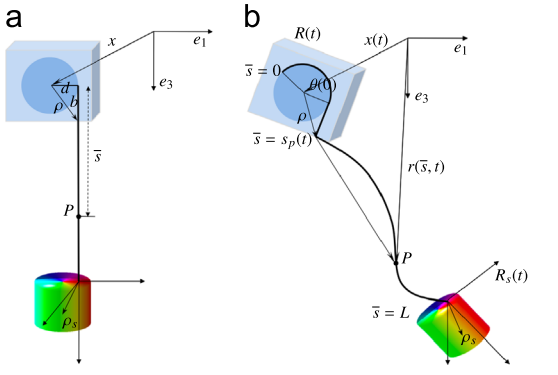

Fig. 1. Tethered spacecraft model. (a) Reference configuration and (b) deformed configuration.

$J \in \mathbb{R}^{3\times3}$ the inertia matrix of the base spacecraft

$R \in \mathrm{SO}(3)$ the rotation matrix from the first body-fixed frame to the reference frame

$\Omega \in \mathbb{R}^3$ the angular velocity of the base spacecraft represented in its body-fixed frame

$\mathrm{x} \in \mathbb{R}^3$ the location of the center of mass of the base spacecraft represented in the global reference frame

$d \in \mathbb{R}$ the radius of the reeling drum

$b \in \mathbb{R}$ the length of the guideway

$\rho \in \mathbb{R}^3$ the vector from the center of mass of the base spacecraft to the beginning of the guideway represented in its body-fixed frame, $\rho = [d, 0, b]$.

$m_r \in \mathbb{R}$ the mass of the reeling drum

$J_r \in \mathbb{R}^{3\times3}$ the inertia matrix of the reeling drum, $J_r = \kappa_r d^2$ for a matrix $\kappa_r \in \mathbb{R}^{3\times3}$

$L \in \mathbb{R}$ the total unstretched length of the tether

$\bar{s} \in [0, L]$ the unstretched arc length of the tether between the point at which the tether is attached to the reeling drum and a material point P on the tether

$s(\bar{s}, t) \in \mathbb{R}^+$ the stretched arc length of the tether to the material point located at $\bar{s}$

$s_p(t) \in [b, L]$ the arc length of the tether between the point at which the tether is attached to the reeling drum and the beginning of the guideway

$r(\bar{s}, t) \in \mathbb{R}^3$ the deformed location of a material point P from the origin of the global reference frame; $r(s_p, t) = x(t) + R(t)\rho$

$\theta(\bar{s}) \in \mathbb{R}$ $\theta = (s_p - b - \bar{s})/d$ for $\bar{s} \in [0, s_p - b]$

$\bar{\mu} \in \mathbb{R}$ The mass of the tether per unit unstretched length

$m_b \in \mathbb{R}$ the total mass of the base spacecraft, including the reeling mechanism, i.e., $m_b = m + m_r + \bar{\mu} s_p$

$m_s \in \mathbb{R}$ the mass of the sub-spacecraft

$J_s \in \mathbb{R}$ the inertia matrix of the sub-spacecraft

$R_s \in \mathrm{SO}(3)$ the rotation matrix from the second body-fixed frame to the global reference frame

$\Omega_s \in \mathbb{R}^3$ the angular velocity of the sub-spacecraft represented in its body-fixed frame

$\rho_s \in \mathbb{R}^3$ the vector from the point where the tether is attached to the sub-spacecraft to the center of mass of the sub-spacecraft represented in its body-fixed frame

$u \in \mathbb{R}$ control moment applied at the reeling drum

A configuration of this system can be described by the locations of all the material points of the deployed portion of the tether, namely $r(\bar{s}, t)$ for $\bar{s} \in [s_p, L]$, the location and the attitude of the base spacecraft $(x, R) \in \mathrm{SE}(3)$, the attitude of the sub-spacecraft $R_s \in \mathrm{SO}(3)$, and the length of the undeployed portion of the tether, $s_p \in \mathbb{R}$. So, the configuration manifold is $\mathrm{G} = C^\infty([0, L], \mathbb{R}^3) \times \mathrm{SE}(3) \times \mathrm{SO}(3) \times \mathbb{R}$, where $C^\infty([0, L], \mathbb{R}^3)$ denotes the space of smooth connected curve segments on $\mathbb{R}^3$, $\mathrm{SO}(3) = \{R \in \mathbb{R}^{3\times3} \mid R^T R = I, \det[R] = 1\}$, and $\mathrm{SE}(3) = \mathbb{R}^3 \circledS \mathrm{SO}(3)$ [19].

Throughout this paper, we assume that (i) the radius of a reeling drum and the length of a guideway is small compared to the length of a tether; (ii) the reeling drum rotates about the second axis of the first body-fixed frame attached to the base spacecraft; (iii) the deployed portion of the tether is extensible, but the portion of the tether on

the reel and the guideway inside the base spacecraft is inextensible; (iv) the gravity is uniform over the base spacecraft and the sub-spacecraft.

The attitude kinematics equation of the base spacecraft and the sub-spacecraft is given by

$$\dot{R} = R\hat{\Omega}, \quad \dot{R}_s = R\hat{\Omega}_s, \tag{1}$$

where the *hat map* $\hat{\cdot}: \mathbb{R}^3 \to \mathfrak{so}(3)$ is defined by the condition that $\hat{x}y = x \times y$ for any $x, y \in \mathbb{R}^3$ [18]. The inverse of the hat map is denoted by the *vee* map: $(\cdot)^\wedge : \mathfrak{so}(3) \to \mathbb{R}^3$.

3. Continuous-time analytical model

In this section, we develop continuous-time equations of motion for a tethered spacecraft using Hamilton's variational principle.

3.1. Lagrangian

Kinetic energy: The kinetic energy is composed of the kinetic energy of the base rigid body T_{b_1}, the kinetic energy of the reeling mechanism T_{b_2}, the kinetic energy of the deployed portion of the tether T_t, and the kinetic energy of the sub-spacecraft T_s. The kinetic energy of the base rigid body is given by

$$T_{b_1} = \tfrac{1}{2} m \dot{x} \cdot \dot{x} + \tfrac{1}{2} \Omega \cdot J \Omega. \tag{2}$$

The kinetic energy of the reeling mechanism is given by

$$T_{b_2} = \tfrac{1}{2} (m_r + \bar{\mu} s_p) \dot{x} \cdot \dot{x} + \tfrac{1}{2} \bar{\mu} s_p \dot{s}_p^2 + \tfrac{1}{2} \kappa_2 \dot{s}_p^2, \tag{3}$$

where $\kappa_2 = e_2 \cdot \kappa_r e_2$. This is obtained by integrating the infinitesimal kinetic energy of the material points on the undeployed portion of tether, and ignoring higher-order terms of b, d due to the assumption that the radius of reeling drum d and the length of the guideway b is much less than the length of the tether.

Let $\dot{r}(\bar{s}, t)$ be the partial derivative of $r(\bar{s}, t)$ with respect to t. The kinetic energy of the deployed portion of the tether is given by

$$T_t = \int_{s_p}^{L} \frac{1}{2} \bar{\mu} \dot{r}(\bar{s}) \cdot \dot{r}(\bar{s}) \, d\bar{s}. \tag{4}$$

Let $\tilde{\rho} \in \mathbb{R}^3$ be the vector from the end of the tether to a mass element of the sub-spacecraft represented with respect to its body-fixed frame. The location of the mass element in the global reference frame is given by $r(L) + R_s \tilde{\rho}$. Then, the kinetic energy of the sub-spacecraft is given by

$$\begin{aligned} T_s &= \int_{\mathcal{B}_s} \frac{1}{2} \| \dot{r}(L) + R_s \hat{\Omega}_s \tilde{\rho} \|^2 \, dm \\ &= \frac{1}{2} m_s \dot{r}(L) \cdot \dot{r}(L) + m_s \dot{r}(L) \cdot R_s \hat{\Omega}_s \rho_s + \frac{1}{2} \Omega_s \cdot J_s \Omega_s. \end{aligned} \tag{5}$$

Here, we use the fact that $\int_{\mathcal{B}_s} \tilde{\rho} \, dm = \rho_c$, and $J_s = -\int_{\mathcal{B}_s} \hat{\rho}_s^2 \, dm$. The total kinetic energy is given by $T = T_{b_1} + T_{b_2} + T_t + T_s$.

Potential energy: From the assumption that the reeling drum is small relative to the length of the tether, the gravitational potential of the base spacecraft and the reeling mechanism can be approximated as follows:

$$V_b = -(m + m_r + \bar{\mu} s_p) \frac{GM}{\|x\|} = -m_b \frac{GM}{\|x\|}, \tag{6}$$

where the gravitational constant and the mass of the Earth are denoted by G and M, respectively.

The strain of the tether at a material point located at $r(\bar{s})$ is given by

$$\epsilon = \lim_{\Delta\bar{s} \to 0} \frac{\Delta s(\bar{s}) - \Delta s}{\Delta \bar{s}} = s'(\bar{s}) - 1,$$

where $()'$ denotes the partial derivative with respect to $\bar{s}$. The tangent vector at the material point is given by

$$e_t = \frac{\partial r(\bar{s})}{\partial s} = \frac{\partial r(\bar{s})}{\partial \bar{s}} \frac{\partial \bar{s}}{\partial s(\bar{s})} = \frac{r'(\bar{s})}{s'(\bar{s}).}$$

Since this tangent vector has unit length, we have $s'(\bar{s}) = \|r'(\bar{s})\|$. Therefore, the strain can be written as $\epsilon = \|r'(\bar{s})\| - 1$. Using this, the elastic potential and the gravitational potential of the deployed portion of the tether are given by

$$V_t = \tfrac{1}{2} \int_{s_p}^{L} EA(\|r'(\bar{s})\| - 1)^2 \, d\bar{s} - \int_{s_p}^{L} \bar{\mu} \frac{GM}{\|r(\bar{s})\|} \, d\bar{s}, \tag{7}$$

where E and A denote Young's modulus and the sectional area of the tether, respectively.

The location of the center of mass of the sub-spacecraft is $r(L) + R_s \rho_s$ in the global reference frame. Since we assume that the gravity is uniform over each spacecraft body, the gravitational potential energy of the sub-spacecraft is given by

$$V_s = -m_s \frac{GM}{\|r(L) + R_s \rho_s\|}. \tag{8}$$

From (2)–(8), the Lagrangian of the tethered spacecraft is given by

$$L = (T_{b_1} + T_{b_2} - V_b) + (T_t - V_t) + (T_s - V_s) \tag{9}$$

$$L = L_b + L_t + L_s. \tag{10}$$

3.2. Euler–Lagrange equations

Let the action integral be

$$\mathfrak{G} = \int_{t_0}^{t_f} L_b + L_t + L_s \, dt = \mathfrak{G}_b + \mathfrak{G}_t + \mathfrak{G}_s. \tag{11}$$

According to the Lagrange–d'Alembert principle, the variation of the action integral is equal to the negative of the virtual work for fixed boundary conditions, which yields the forced Euler–Lagrange equations. For the given tethered spacecraft model, there are three aspects that require careful consideration: (i) the rotation matrices R, R_s that represents the attitudes lie in the nonlinear Lie group SO(3); (ii) the domain of the integral depends on the variable $s_p(t)$ at (4); (iii) since the tether is assumed to be inextensible in the guideway, and it is extensible outsize of the guideway, there exists a discontinuity in strain at the beginning of the guideway.

Variation of $\mathfrak{G}_b$: The attitudes of spacecraft are represented by the rotation matrix $R, R_s \in \mathrm{SO}(3)$. Therefore, the

variation of the rotation matrix should be consistent with the geometry of the special orthogonal group. In [18], it is expressed in terms of the exponential map as

$$\delta R = \left.\frac{d}{d\epsilon}\right|_{\epsilon=0} R^{\epsilon} = \left.\frac{d}{d\epsilon}\right|_{\epsilon=0} R\exp\epsilon\hat{\eta} = R\hat{\eta}, \tag{12}$$

for $\eta \in \mathbb{R}^3$. The key idea is expressing the variation of a Lie group element in terms of a Lie algebra element. This is desirable since the Lie algebra $so(3)$ of the special orthogonal group, represented by 3×3 skew-symmetric matrices, is isomorphic as a Lie algebra to $\mathbb{R}^3$. As a result, the variation of the three-dimensional rotation matrix R is expressed in terms of a vector $\eta \in \mathbb{R}^3$. We can directly show that (12) satisfies $\delta(R^TR) = \delta R^T R + R^T\delta R = -\hat{\eta}+\hat{\eta} = 0$. The corresponding variation of the angular velocity is obtained from the kinematics equation (1):

$$\delta\hat{\Omega} = \left.\frac{d}{d\epsilon}\right|_{\epsilon=0} (R^{\epsilon})^T\dot{R}^{\epsilon} = (\dot{\eta}+\Omega\times\eta)^{\wedge}. \tag{13}$$

Using (12) and (13), and integration by parts, the variation of $\mathfrak{G}_b$ is given by

$$\begin{aligned}\delta\mathfrak{G}_b = &\int_{t_0}^{t_f}\left\{-m_b\ddot{x} - \overline{\mu}\dot{s}_p\dot{x} - GMm_b\frac{x}{\|x\|^3}\right\}\cdot\delta x\\ &+\left\{-(\overline{\mu}s_p+\kappa_2)\ddot{s}_p + \tfrac{1}{2}\overline{\mu}\left(\dot{x}\cdot\dot{x} - \dot{s}_p^2 + 2\frac{GM}{\|x\|}\right)\right\}\delta s_p\\ &-\{J\dot{\Omega}+\hat{\Omega}J\Omega\}\cdot\eta\, dt.\end{aligned} \tag{14}$$

Variation of $\mathfrak{G}_t$: The action integral for tether namely $\mathfrak{G}_t$ is expressed as a double integral on $(t,\overline{s}) \in [t_0,t_f]\times[s_p(t),L]$, given by

$$\mathfrak{G}_t = \int_{t_0}^{t_f}\int_{s_p(t)}^{L}\frac{1}{2}\overline{\mu}\dot{r}(\overline{s})\cdot\dot{r}(\overline{s}) - \frac{1}{2}EA(\|r'(\overline{s})\|-1)^2 + \overline{\mu}\frac{GM}{\|r(\overline{s})\|}d\overline{s}\, dt.$$

Thus, its variation should take account of the $s_p(t)$ variation:

$$\begin{aligned}\delta\mathfrak{G}_t = &\int_{t_0}^{t_f}\int_{s_p}^{L}\overline{\mu}\dot{r}(\overline{s})\cdot\delta\dot{r}(\overline{s}) - EA\frac{\|r'(\overline{s})\|-1}{\|r'(\overline{s})\|r'(\overline{s})\cdot\delta r'(\overline{s})}\\ &-\overline{\mu}GM\frac{r(\overline{s})}{\|r(\overline{s})\|^3}\cdot\delta r(\overline{s})\, d\overline{s}\, dt - \int_{t_0}^{t_f}\left\{\frac{1}{2}\overline{\mu}\dot{r}\left(s_p^+\right)\cdot\dot{r}\left(s_p^+\right)\cdot\right.\\ &\left.-\frac{1}{2}EA(\|r'(s_p^+)\|-1)^2 + \overline{\mu}\frac{GM}{\|r(s_p)\|}\right\}\delta s_p\, dt,\end{aligned} \tag{15}$$

where $\dot{r}(s_p^+)$ represents the material velocity at the outside of the guideway.

Now, we focus on the first term of (15). We cannot apply integration by parts with respect to $\overline{s}$, since the order of the integrals cannot be interchanged as $s_p(t)$ depends on t. Instead, we use Green's theorem [15]:

$$\oint_{\mathcal{C}}\dot{r}(\overline{s})\cdot\delta r(\overline{s})\, d\overline{s} = \int_{t_0}^{t_f}\int_{s_p}^{L}\frac{d}{dt}(\dot{r}(\overline{s})\cdot\delta r(\overline{s}))\, d\overline{s}\, dt, \tag{16}$$

where $\oint_{\mathcal{C}}$ represents the counterclockwise line integral on the boundary $\mathcal{C}$ of the region $[t_0,t_f]\times[s_p(t),L]$. The boundary $\mathcal{C}$ is composed of four lines: $(t=t_0, \overline{s}\in[s_p(t_0),L])$, $(t=t_f, \overline{s}\in[s_p(t_f),L])$, $(t\in[t_0,t_f], \overline{s}=s_p(t))$, and $(t\in[t_0,t_f], \overline{s}=L)$. For the first two lines, $\delta r(\overline{s})=0$ since $t=t_0,t_f$. For the last line, $d\overline{s}=0$ since $\overline{s}$ is fixed. Thus, parameterizing the third line by t, we obtain

$$\oint_{\mathcal{C}}\dot{r}(\overline{s})\cdot\delta r(\overline{s})\, d\overline{s} = \int_{t_0}^{t_f}\dot{r}(s_p(t))\cdot\delta r(s_p(t))\dot{s}_p(t)\, dt.$$

Substituting this into (16) and rearranging, we obtain

$$\begin{aligned}&\int_{t_0}^{t_f}\int_{s_p}^{L}\dot{r}(\overline{s})\cdot\delta\dot{r}(\overline{s})\, d\overline{s}\, dt\\ &= \int_{t_0}^{t_f}\left[\int_{s_p}^{L} -\ddot{r}(\overline{s})\cdot\delta r(\overline{s})\, d\overline{s} + \dot{r}(s_p)\cdot\delta r(s_p)\dot{s}_p\right] dt.\end{aligned} \tag{17}$$

Substituting (17) into (15), and using integration by parts, the variation of $\mathfrak{G}_t$ can be written as

$$\begin{aligned}\delta\mathfrak{G}_t = &\int_{t_0}^{t_f}\int_{s_p}^{L}\left\{-\overline{\mu}\ddot{r}(\overline{s}) + F'(\overline{s}) - \overline{\mu}GM\frac{r(\overline{s})}{\|r(\overline{s})\|^3}\right\}\cdot\delta r(\overline{s})\, d\overline{s}\, dt\\ &+\int_{t_0}^{t_f}\left\{-\frac{1}{2}\overline{\mu}\dot{r}\left(s_p^+\right)\cdot\dot{r}\left(s_p^+\right) + \tfrac{1}{2}EA(\|r'(s_p^+)\|-1)^2\right.\\ &\left.-\overline{\mu}\frac{GM}{\|r(s_p)\|}\right\}\delta s_p\\ &+\overline{\mu}\dot{r}(s_p^+)\cdot\delta r(s_p^+)\dot{s}_p - F(L)\cdot\delta r(L) + F(s_p)\cdot\delta r(s_p^+)\, dt,\end{aligned} \tag{18}$$

where $F(\overline{s}) = EA((\|r'(\overline{s})\|-1)/\|r'(\overline{s})\|)r'(\overline{s})$.

This is further simplified as follows. Let $r_p = r(s_p(t),t)$ be the location of the beginning of the guideway. Since it can be written as $r_p = x+R\rho$, we have $\delta r_p = \delta r(s_p^+)+r'(s_p^+)\delta s_p = \delta x + R\hat{\eta}\rho$. Thus,

$$\delta r(s_p^+) = -r'(s_p^+)\delta s_p + \delta x - R\hat{\rho}\eta.$$

Similarly, we obtain

$$\dot{r}(s_p^+) = -r'(s_p^+)\dot{s}_p + \dot{x} - R\hat{\rho}\Omega.$$

Substituting these into (18), the variation of $\mathfrak{G}_t$ is expressed in terms of $\delta r(\overline{s})$, δs_p, δx, η, and $\delta r(L)$.

Variation of $\mathfrak{G}_s$: Similar to (14), the variation of $\mathfrak{G}_s$ is given by

$$\begin{aligned}\delta\mathfrak{G}_s = &\int_{t_0}^{t_f}\left\{-m_s\ddot{r}(L) - m_sR_s\hat{\Omega}_s^2\rho_s - m_sR_s\hat{\dot{\Omega}}_s\rho_s\right.\\ &\left.-GMm_s\frac{r(L)+R_s\rho_s}{\|r(L)+R_s\rho_s\|^3}\right\}\cdot r(L) + \left\{-J\dot{\Omega}_s - m_s\hat{\rho}_sR_s^T\ddot{r}(L)\right.\\ &\left.-\hat{\Omega}_sJ\Omega_s - GMm_s\frac{r(L)+R_s\rho_s}{\|r(L)+R_s\rho_s\|^3}\right\}\cdot\eta_s\, dt.\end{aligned} \tag{19}$$

In short, the variation of the action integral is given by (14), (18), and (19).

Variational principle with discontinuity: Let $r(s_p^-)$, and $r(s_p^+)$ be the material point of the tether just inside the guideway, and the material point just outside the guideway, respectively. Since the tether is inextensible inside the guideway, $\|r'(s_p^-)\| = 1$. Since the tether is extensible outside the guideway, $\|r'(s_p^+)\| = 1+\epsilon^+$, where ϵ^+ represents the strain of the tether just outside the guideway. Due to this discontinuity, the speed of the tether changes instantaneously by the amount $\epsilon^+|\dot{s}_p|$ at the guideway.

As a result, the variation of the action integral is not equal to the negative of the virtual work done by the external control moment u at the reeling drum. Instead, an additional term Q, referred to as Carnot energy loss term,

should be introduced [13,20]. The resulting variational principle is given by

$$\delta\mathfrak{G}+\int_{t_0}^{t_f}(Q+u/d)\delta s_p-ue_2\cdot\eta\,dt=0. \tag{20}$$

The corresponding time rate of change of the total energy is given by $\dot{E}=(Q+u/d)\dot{s}_p$, where the first term $Q\dot{s}_p$ represents the energy dissipation rate due to the velocity and the strain discontinuity. The corresponding expression for Q has been developed in [15]

$$Q=-\tfrac{1}{2}\overline{\mu}(\|r'(s_p^+)\|-1)^2\dot{s}_p^2-\tfrac{1}{2}EA(\|r'(s_p^+)\|-1)^2. \tag{21}$$

Euler–Lagrange equations: Using these results, and the variational principle with discontinuity (20), we obtain the Euler–Lagrange equations for the given tethered spacecraft model in (22)–(27). In (25), we require that $r(s_p)=x+R\rho$ for the continuity of the tether.

These equations provide a comprehensive, analytical model of tethered spacecraft, including rotational dynamics of spacecraft, deformation of tether, and reeling mechanism. We have shown that the equation of motions can be derived based on a variational principle in a unified way. These can be simplified in a number of special cases. For example, we can substitute $\dot{s}_p=0$ when the length of the deployed portion of the tether is fixed, and we can set $\rho=\rho_s=0$ when the main spacecraft and the sub-spacecraft are modeled as point masses instead of rigid bodies:

$$-(m+m_r+\overline{\mu}s_p)\ddot{x}-GM(m+m_r+\overline{\mu}s_p)\frac{x}{\|x\|^3}+\overline{\mu}\dot{s}_p(-r'(s_p^+)\dot{s}_p-R\hat{\rho}\Omega)+F(s_p)=0, \tag{22}$$

$$-J\dot{\Omega}-\hat{\Omega}J\Omega+\overline{\mu}\dot{s}_p\hat{\rho}R^T(-r'(s_p^+)\dot{s}_p+\dot{x}-R\hat{\rho}\Omega)+\hat{\rho}R^TF(s_p)-ue_2=0, \tag{23}$$

$$-(\overline{\mu}s_p+\kappa_2)\ddot{s}_p-\frac{1}{2}\overline{\mu}(\dot{x}-R\hat{\rho}\Omega)\cdot(\dot{x}-R\hat{\rho}\Omega)+\frac{1}{2}\overline{\mu}\dot{x}\cdot\dot{x}-\overline{\mu}\frac{GM}{\|r(s_p)\|}+\overline{\mu}\frac{GM}{\|x\|}-F(s_p)\cdot r'\left(s_p^+\right)+\overline{\mu}\dot{s}_p^2\left(\|r'\left(s_p^+\right)\|-1\right)+\frac{u}{d}=0, \tag{24}$$

$$-\overline{\mu}\ddot{r}(\overline{s})+F'(\overline{s})-\overline{\mu}GM\frac{r(\overline{s})}{\|r(\overline{s})\|}=0,\quad(\overline{s}\in[s_p,L],\ r(s_p)=x+R\rho), \tag{25}$$

$$-m_s\ddot{r}(L)+m_sR_s\hat{\rho}_s\dot{\Omega}_s-m_sR_s\hat{\Omega}_s^2\rho_s-GMm_s\frac{r(L)+R_s\rho_s}{\|r(L)+R_s\rho_s\|^3}-F(L)=0, \tag{26}$$

$$-J_s\dot{\Omega}_s-m_s\hat{\rho}_sR_s^T\ddot{r}(L)-\hat{\Omega}_sJ_s\Omega_s-GMm_s\hat{\rho}_sR_s^T\frac{r(L)+R_s\rho_s}{\|r(L)+R_s\rho_s\|^3}=0, \tag{27}$$

where $F(\overline{s})=EA((\|r'(\overline{s})\|-1)/\|r'(\overline{s})\|)r'(\overline{s})$ denotes the tension of the tether.

4. Lie group variational integrator

The Euler–Lagrange equations developed in the previous section provide an analytical model for a tethered spacecraft. However, the standard finite-difference approximations or finite-element approximations of those equations using general purpose numerical integrators may not preserve the geometric properties of the system accurately [17]. For example, it has been shown that a general purpose numerical integrator fails to compute the energy dissipation rate correctly [21], and that explicit Runge–Kutta methods do not preserve the orthogonal structure of rotation matrices, thereby yielding unreliable numerical results for the rotational dynamics of a rigid body [22,23].

Geometric numerical integrators deal with numerical integration techniques that preserve the underlying geometric properties of a dynamical system, such as invariants, symmetries, or the structure of configuration manifolds [17,24]. Variational integrators provide a systematic method to construct geometric numerical integrators for mechanical systems [21], where a numerical integrator is developed according to a discrete analogue of Hamilton's variational principle. Numerical flows of variational integrators can have desirable properties such as second-order accuracy, symplecticity and momentum preservation, and they can exhibit good energy behavior over a long time period.

In particular, Lie group variational integrators are developed for Lagrangian/Hamiltonian systems evolving on a Lie group [18]. They inherit the desirable computational properties of variational integrators, and they also preserve the Lie group structures of a configuration manifold naturally by updating a group element using the group operation. These are in contrast to projection-based methods where projection at each time-step may corrupt conservation properties, or constrained-based methods where a nonlinear constraint needs to be solved at each time-step. They also avoid singularities introduced by local parameterizations of a Lie group.

The unique feature of Lie group variational integrators is that they preserve both the symplecticity of mechanical systems and the nonlinear structure of a Lie group configuration manifold concurrently, and it has been shown that this is critical for accurate and efficient simulations of multibody dynamics [23].

In this section, we develop a Lie group variational integrator for a tethered spacecraft. We first discretize the tether using a finite-element model, and we construct a discrete Lagrangian, which is used to derive the discrete Euler–Lagrange equations for tethered spacecrafts.

4.1. Discretized tethered spacecraft model

Let $h>0$ be a fixed time-step. The value of variables at $t=t_0+kh$ is denoted by a subscript k. We discretize the deployed portion of the tether using N identical line elements. Since the unstretched length of the deployed portion of the tether is $L-s_{p_k}$, the unstretched length of each element is $l_k=(L-s_{p_k})/N$. Let the subscript a denote the variables related to the a-th element. The natural coordinate on the a-th element is defined by

$$\zeta_{k,a}(\overline{s})=\frac{(\overline{s}-s_{p_k})-(a-1)l_k}{l_k} \tag{28}$$

for $\overline{s}\in[s_{p_k}+(a-1)l_k,s_{p_k}+al_k]$. This varies between 0 and 1 on the a-th element. Let S_0 and S_1 be shape functions given

by $S_0(\zeta)=1-\zeta$, and $S_1(\zeta)=\zeta$, respectively. These shape functions are also referred to as *tent functions*.

Using this finite-element model, the position vector $r(\bar{s},t)$ of a material point in the a-th element is approximated as follows:

$$r_k(\bar{s})=S_0(\zeta_{k,a})r_{k,a}+S_1(\zeta_{k,a})r_{k,a+1}. \tag{29}$$

Therefore, a configuration of the discretized tethered spacecraft at $t=kh+t_0$ is described by $g_k=(x_k;R_k;s_{p_k};r_{k,1},\ldots,r_{k,N+1};R_{s_k})$, and the corresponding configuration manifold is $\mathsf{G}=\mathbb{R}^3\times \mathrm{SO}(3)\times\mathbb{R}\times(\mathbb{R}^3)^{N+1}\times\mathrm{SO}(3)$. This is a Lie group where the group acts on itself by the diagonal action [19]: the group action on x_k, s_{p_k}, and $r_{k,a}$ is addition, and the group action on R_k, R_{s_k} is matrix multiplication.

We define a discrete-time kinematics equation using the group action as follows. Define $f_k=(\Delta x_k;F_k;\Delta s_{p_k};\Delta r_{k,1},\ldots,\Delta r_{k,N+1};F_{s_k})\in\mathsf{G}$ such that $g_{k+1}=g_kf_k$:

$$\begin{aligned}&(x_{k+1};R_{k+1};s_{p_{k+1}};r_{k+1,a};R_{k+1})\\&\quad=(x_k+\Delta x_k;R_kF_k;s_{p_k}+\Delta s_{p_k};r_{k,a}+\Delta r_{k,a};R_{s_k}F_{s_k}).\end{aligned} \tag{30}$$

Therefore, $f_k\in\mathsf{G}$ represents the relative update between two integration steps. This ensures that the structure of the Lie group configuration manifold is numerically preserved since g_k is updated by f_k using the right Lie group action of G on itself.

4.2. Discrete Lagrangian

A discrete Lagrangian $L_d(g_k,f_k):\mathsf{G}\times\mathsf{G}\to\mathbb{R}$ is an approximation of the Jacobi solution of the Hamilton–Jacobi equation, which is given by the integral of the Lagrangian along the exact solution of the Euler–Lagrange equations over a single time-step:

$$L_d(g_k,f_k)\approx\int_0^h L(\tilde{g}(t),\tilde{g}^{-1}(t)\dot{\tilde{g}}(t))\,dt,$$

where $\tilde{g}(t):[0,h]\to\mathsf{G}$ satisfies Euler–Lagrange equations with boundary conditions $\tilde{g}(0)=g_k$, $\tilde{g}(h)=g_kf_k$. The resulting discrete-time Lagrangian system, referred to as a variational integrator, approximates the Euler–Lagrange equations to the same order of accuracy as the discrete Lagrangian approximates the Jacobi solution [21].

We construct a discrete Lagrangian for the tethered spacecraft using the trapezoidal rule. From the attitude kinetics equations (1), the angular velocity is approximated by

$$\hat{\Omega}_k\approx\frac{1}{h}R_k^T(R_{k+1}-R_k)=\frac{1}{h}(F_k-I).$$

Define a non-standard inertia matrix $J_d=\frac{1}{2}\,\mathrm{tr}[J]I-J$. Using the trace operation and the non-standard inertia matrix, the rotational kinetic energy of the main spacecraft at (2) can be written in terms of $\hat{\Omega}$ as $\frac{1}{2}\Omega\cdot J\Omega=\frac{1}{2}\,\mathrm{tr}\left[\hat{\Omega}J_d\hat{\Omega}^T\right]$. Using this, and (2), (3), the kinetic energy of the base spacecraft is given by

$$\begin{aligned}T_{k,b}&=\frac{1}{2h^2}(m+m_r+\bar{\mu}s_{p_k})\Delta x_k\cdot\Delta x_k+\frac{1}{2h^2}(\bar{\mu}s_{p_k}+\kappa_s)\Delta s_{p_k}^2\\&\quad+\frac{1}{h^2}\,\mathrm{tr}[(I-F_k)J_d],\end{aligned} \tag{31}$$

where we use properties of the trace operator: $\mathrm{tr}[AB]=\mathrm{tr}[BA]=\mathrm{tr}[A^TB^T]$ for any matrices $A,B\in\mathbb{R}^{3\times3}$.

Next, we find the kinetic energy of the tether. Using the chain rule, the partial derivative of $r_k(\bar{s})$, given by (29), with respect to t is given by

$$\begin{aligned}\dot{r}_k(s)=\frac{1}{h}\Bigg\{&S_0(\zeta_{k,a})\Delta r_{k,a}+S_1(\zeta_{k,a})\Delta r_{k,a+1}\\&+\frac{(L-s)}{(L-s_{p_k})}\frac{(r_{k,a}-r_{k,a+1})}{l_k}\Delta s_{p_k}\Bigg\}.\end{aligned}$$

Substituting this into (4), the contribution of the a-th tether element to the kinetic energy of the tether is given by

$$\begin{aligned}T_{k,a}&=\int_0^1\frac{1}{2}\mu l_k\|\dot{r}_k(\zeta_{k,a})\|^2\,d\zeta_{k,a}\\&=\frac{1}{2h^2}M_k^1\Delta r_{k,a}\cdot\Delta r_{k,a}+\frac{1}{2h^2}M_k^2\Delta r_{k,a+1}\cdot\Delta r_{k,a+1}\\&\quad+\frac{1}{2h^2}M_{k,a}^3\Delta s_{p_k}^2+\frac{1}{h^2}M_k^{12}\Delta r_{k,a}\cdot\Delta r_{k,a+1}\\&\quad+\frac{1}{h^2}M_{k,a}^{23}\Delta s_{p_k}\cdot\Delta r_{k,a+1}+\frac{1}{h^2}M_{k,a}^{31}\Delta s_{p_k}\cdot\Delta r_{k,a},\end{aligned} \tag{32}$$

where inertia matrices are given by

$$\begin{aligned}&M_k^1=\frac{1}{3}\bar{\mu}l_k,\quad M_k^2=M_k^1,\\&M_{k,a}^3=\frac{1}{3}\bar{\mu}l_k\frac{(3N^2+3N+1-6Na-3a+3a^2)}{N^2},\\&M_k^{12}=\frac{1}{6}\bar{\mu}l_k,\quad M_{k,a}^{23}=\frac{1}{6}\bar{\mu}\frac{(1+3N-3a)}{N}(r_{k,a}-r_{k,a+1}),\\&M_{k,a}^{31}=\frac{1}{6}\bar{\mu}\frac{(2+3N-3a)}{N}(r_{k,a}-r_{k,a+1}).\end{aligned}$$

Similar to (31), from (5), the kinetic energy of the sub-spacecraft is given by

$$\begin{aligned}T_{k,s}&=\frac{1}{2h^2}m_s\Delta r_{k,N+1}\cdot\Delta r_{k,N+1}+\frac{1}{h^2}\,\mathrm{tr}\left[(I-F_{s_k})J_{s_d}\right]\\&\quad+\frac{1}{h^2}m_s\Delta r_{k,N+1}\cdot R_{s_k}(F_{s_k}-I)\rho_s.\end{aligned} \tag{33}$$

From (31), (32), and (33), the total kinetic energy of the discretized tethered spacecraft is given by

$$T_k=T_{k,b}+\sum_{a=1}^{N}T_{k,a}+T_{k,s}. \tag{34}$$

Similarly, from (6), (7), and (8), the total potential energy is given by

$$\begin{aligned}V_k=&-GM(m+m_r+\bar{\mu}s_{p_k})\frac{1}{\|x_k\|}\\&+\sum_{a=1}^{N}-2GM\bar{\mu}l_k\frac{1}{\|r_{k,a}+r_{k,a+1}\|}\\&+\frac{1}{2}\frac{EA}{l_k}(\|r_{k,a+1}-r_{k,a}\|-l_k)^2-GMm_s\frac{1}{\|r_{k,N+1}+R_{s_k}\rho_s\|}.\end{aligned} \tag{35}$$

Using (34) and (35), we choose the discrete Lagrangian of the discretized tethered spacecraft to be

$$L_{d_k}(g_k,f_k)=hT_k(g_k,f_k)-\frac{h}{2}V_k(g_k,f_k)-\frac{h}{2}V_{k+1}(g_k,f_k). \tag{36}$$

This corresponds to an approximation to the action integral given by (11) over a single time-step, with second-order accuracy as it is based on the trapezoidal rule. It can be shown that the resulting variational integrator will have the same second-order accuracy [21].

4.3. Discrete-time Euler–Lagrange equations

We define the discrete action sum $\mathfrak{G}_d = \sum_{k=1}^{n} L_{d_k}(g_k, f_k)$. According to the discrete Lagrange–d'Alembert principle, the variation of the action sum is equal to the negative of the discrete virtual work. This yields the discrete-time forced Euler–Lagrange equations, which we call a variational integrator.

In [18], the following Lie group variational integrator has been developed for Lagrangian systems on an arbitrary Lie group:

$$\begin{aligned}&\mathsf{T}_e^*\mathsf{L}_{f_{k-1}} \cdot \mathbf{D}_{f_{k-1}} L_{d_{k-1}} - \mathrm{Ad}^*_{f_k^{-1}} \cdot (\mathsf{T}_e^*\mathsf{L}_{f_k} \cdot \mathbf{D}_{f_k} L_{d_k}) \\ &\quad + \mathsf{T}_e^*\mathsf{L}_{g_k} \cdot \mathbf{D}_{g_k} L_{d_k} + U_{d_k} + Q_{d_k} = 0, \end{aligned} \tag{37}$$

$$g_{k+1} = g_k f_k, \tag{38}$$

where $\mathsf{TL} : \mathsf{TG} \to \mathsf{TG}$ is the tangent map of the left translation, $\mathbf{D}_f$ represents the derivative with respect to f, and $\mathrm{Ad}^* : \mathsf{G} \times \mathfrak{g}^* \to \mathfrak{g}^*$ is the co-Ad operator [19].

The virtual work due to the control input and the Carnot energy loss are denoted by $U_{d_k} \in \mathfrak{g}^*$ and $Q_{d_k} \in \mathfrak{g}^*$, respectively, and they are chosen to be

$$U_{d_k} \cdot (g^{-1}\delta g_k) = \frac{h}{d} u_k \delta s_{p_k} - h u_k e_2 \cdot \eta_k, \tag{39}$$

$$\begin{aligned} Q_{d_k} \cdot (g^{-1}\delta g_k) = &-\frac{h}{2l_k^2}\left(\bar{\mu}\Delta s_{p_k}^2/h^2 + EA\right) \\ &\times (\|r_{k,2} - r_{k,1}\| - l_k)^2 \ \delta s_{p_k}. \end{aligned} \tag{40}$$

By substituting (36), (39), and (40) into (37) and (38), we obtain a Lie group variational integrator for the given discrete tethered spacecraft model. This involves deriving the derivatives of the discrete Lagrangian and their cotangent lift. More details about the derivation and the resulting Lie group variational integrators are summarized in the Appendix, which also includes a description of the computational approach.

Computational properties: One of the desirable computational properties of the proposed Lie group variational integrator is that it is developed directly on the special orthogonal group, using rotation matrices. It is well known that local parameterizations of SO(3), such as Euler angles or Rodrigues parameters, have singularities. Therefore, they are not suitable for numerical simulation of complex rotational maneuvers of spacecraft, as one has to continually transform into new local parameterizations in order to avoid the numerical ill-conditioning that arises near the coordinate singularities.

Quaternions do not have singularities but since the group **SU**(2) of quaternions double-covers SO(3), there is an ambiguity in representing attitudes. Furthermore, the unit-length of quaternions is not generally preserved in numerical simulations, and therefore attitudes cannot be determined accurately. In some cases, numerical solutions are obtained by applying a one-step method and projecting onto the unit sphere at each time-step. But, such projections interfere with the desirable long-time properties of numerical integrators, since the projection typically breaks the structure-preservation property, and the errors accumulate over time.

In the proposed approach, rotation matrices are updated using the corresponding group operation, namely matrix multiplication, and therefore the group structure is preserved automatically to the level of machine precision, without the need for projection. This also avoids the singularities and ambiguities that arise in other attitude representations.

Numerical flows of the proposed Lie group variational integrator are symplectic and momentum preserving as it is developed according to Hamilton's variational principle. These ensure long-term structural stability in computational results, and they avoid the artificial numerical dissipation that appears in general purpose numerical integrators. These conservation properties are difficult to achieve in conventional approaches that are based on finite-difference approximations of the continuous equations of motion.

When the reeling mechanism and the rotational dynamics are ignored, i.e., $\Delta s_{p_k} = \rho = \rho_c = 0$, it can be shown that the proposed Lie group variational integrator for the deformation tether dynamics is equivalent to the commonly used explicit central-difference algorithm or the Newmark method (with $\beta = 0$ and $\gamma = \frac{1}{2}$); this integrator has been widely used for numerical simulation of structural dynamics and vibrations [25,26]. This reflects the fact that variational integrators encompass a wide range of structure-preserving integrators as special cases, depending on the choice of the discrete Lagrangian [21]. Consequently, we expect that the wave propagation and tether deformation dynamics computed by the Lie group variational integrator for the tethered spacecraft are second-order accurate and they inherit many of the other good properties of the Newmark class of integrators, including accuracy of amplitudes and frequencies. Due to the complexity of the complete dynamics of the tethered spacecraft, it is not possible to quantify the accuracy properties of the proposed Lie group variational integrator for the combined orbital/attitude dynamics, tether deformation, and reeling mechanism.

5. Numerical example

In this section, computational properties of the Lie group variational integrator are illustrated.

5.1. Validation

The proposed approach is implemented on Matlab and it is first validated by checking that it generates numerical results consistent with a tethered spacecraft model considered in [14]. A case where a sub-spacecraft is released from a stationary base spacecraft under the effects of gravity is considered, and the corresponding detailed simulation parameters are described in [14]. Fig. 2 illustrates the length of tether in the reeling mechanism and

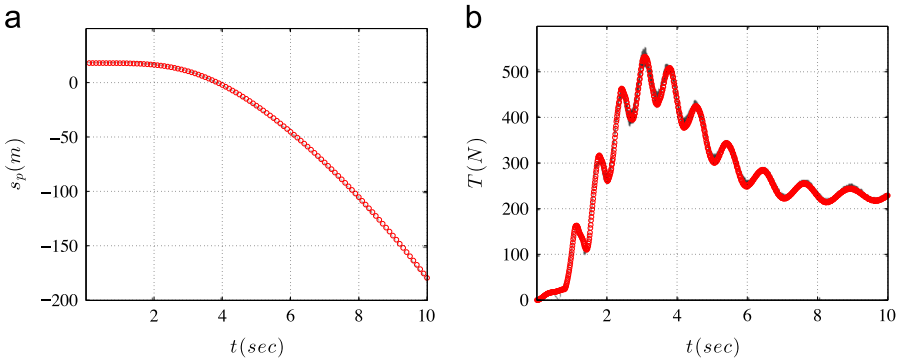

Fig. 2. Validation of algorithm: computational results of the proposed approach (red circles) are compared with a tethered spacecraft model (black) in [14]. (a) Length of tether in the reeling mechanism s_p. (b) Tension at the guideway. (For interpretation of the references to color in this figure caption, the reader is referred to the web version of this paper.)

the tension of tether at the guideway, where the corresponding figure images from the reference [14] are copied as backgrounds. It is shown that the proposed approach (red circles) generates numerical results comparable to [14] (black curves).

5.2. Benchmark study

Next, we perform benchmark studies using the following tethered spacecraft model. The properties of the tethered spacecraft are chosen to be

$$m = 490\ \text{kg}, \quad m_r = 10\ \text{kg}, \quad m_s = 150\ \text{kg},$$
$$l = 120\ \text{km}, \quad \bar{\mu} = 24.7\ \text{kg/km}, \quad EA = 659,700\ \text{N},$$
$$J = \text{diag}[5675.8,\ 5675.8,\ 6125]\ \text{kg m}^2, \quad \rho = [0.5, 0.0, 1]\ \text{m},$$
$$J_s = \text{diag}[500,\ 500,\ 300]\ \text{kg m}^2, \quad \rho_s = [0, 0, 1]\ \text{m}.$$

Initially, the base spacecraft is on a circular orbit with an altitude of 300 km, and the tether and the sub-spacecraft are aligned along the radial direction. The initial unstretched length of the deployed portion of the tether is 20 km, i.e., $s_p(0) = 100$ km. The initial velocity at each point of the tether and the sub-spacecraft is chosen such that it corresponds to the velocity of a circular orbit at that altitude.

We consider the following three cases. In the first case, the reeling drum is fixed so that the length of the deployed portion of the tether is fixed, i.e., $\dot{s}_p \equiv 0$. In the second case, the reeling drum is free to rotate, and the tether is released due to the gravity gradient between the base spacecraft and the sub-spacecraft. The third case is the same as the first case except that the initial velocities of the base spacecraft and the sub-spacecraft are perturbed by about 15% to generate a tumbling motion. For all the cases, the number of tether elements is $N = 20$. The orbital period of a point mass on a circular orbit at the altitude of 300 km is 5410 s.

Simulation results, including time-step, CPU time, and the mean deviation of conserved quantities, are summarized in Table 1. The CPU times are reported for a Matlab implementation on a Macbook Air notebook with Intel Core i5 1.7 GHz processor. For the first case and the third case, we compare the computational properties of the proposed Lie group variational integrator with a Runge–Kutta method: the tether is semi-discretized using the same finite-elements, and the resulting system of continuous-time equations is integrated with an explicit Runge–Kutta method with the same second-order accuracy. They serve to illustrate that the numerical conservation properties of the proposed algorithm are far superior to even a highly resolved Runge–Kutta simulation with time-steps chosen to exceed the computational cost of the proposed Lie group variational integrator. The required computation time can be dramatically reduced by implementing the algorithm using a compiled language such as C, by using fixed-point iterations instead of Newton iterations, and by implementing the method on a parallel computer (see, for example, [27]).

Table 1
Simulation results (LGVI: Lie group variational integrator, RK: Runge–Kutta).

Case	Parameters	LGVI	RK
I	h (s)	0.05	0.003
$t_f = 6000$ s	CPU time (h)	4.15	4.80
	mean$\lvert\Delta E_k\rvert$	7.90×10^{-8}	8.91×10^{-2}
	mean$\lVert I - R_k^T R_k \rVert$	7.38×10^{-14}	4.59×10^{-8}
	mean$\lVert I - R_{s_k}^T R_{s_k} \rVert$	6.11×10^{-14}	7.04×10^{-8}
II	h (s)	0.05	–
$t_f = 3848$ s	CPU time (h)	3.97	–
	mean$\lVert I - R_k^T R_k \rVert$	4.40×10^{-14}	–
	mean$\lVert I - R_{s_k}^T R_{s_k} \rVert$	5.16×10^{-14}	–
III	h (s)	0.01	0.0004
$t_f = 6000$ s	CPU time (h)	24.22	36.17
	mean$\lvert\Delta E_k\rvert$	7.18×10^{-2}	1.89×10^{1}
	mean$\lVert I - R_k^T R_k \rVert$	9.73×10^{-14}	2.30×10^{-3}
	mean$\lVert I - R_{s_k}^T R_{s_k} \rVert$	1.58×10^{-13}	3.14×10^{-2}

Figs. 3–5 illustrate simulation results for each case. We consider a fictitious local vertical, local horizontal (LVLH) frame that is attached to an imaginary spacecraft on a circular orbit with an altitude of 300 km. For each figure, we have the following subfigures: (a) the maneuvers of the tethered spacecraft are illustrated with respect to the LVLH frame. To represent the attitude dynamics of spacecraft,

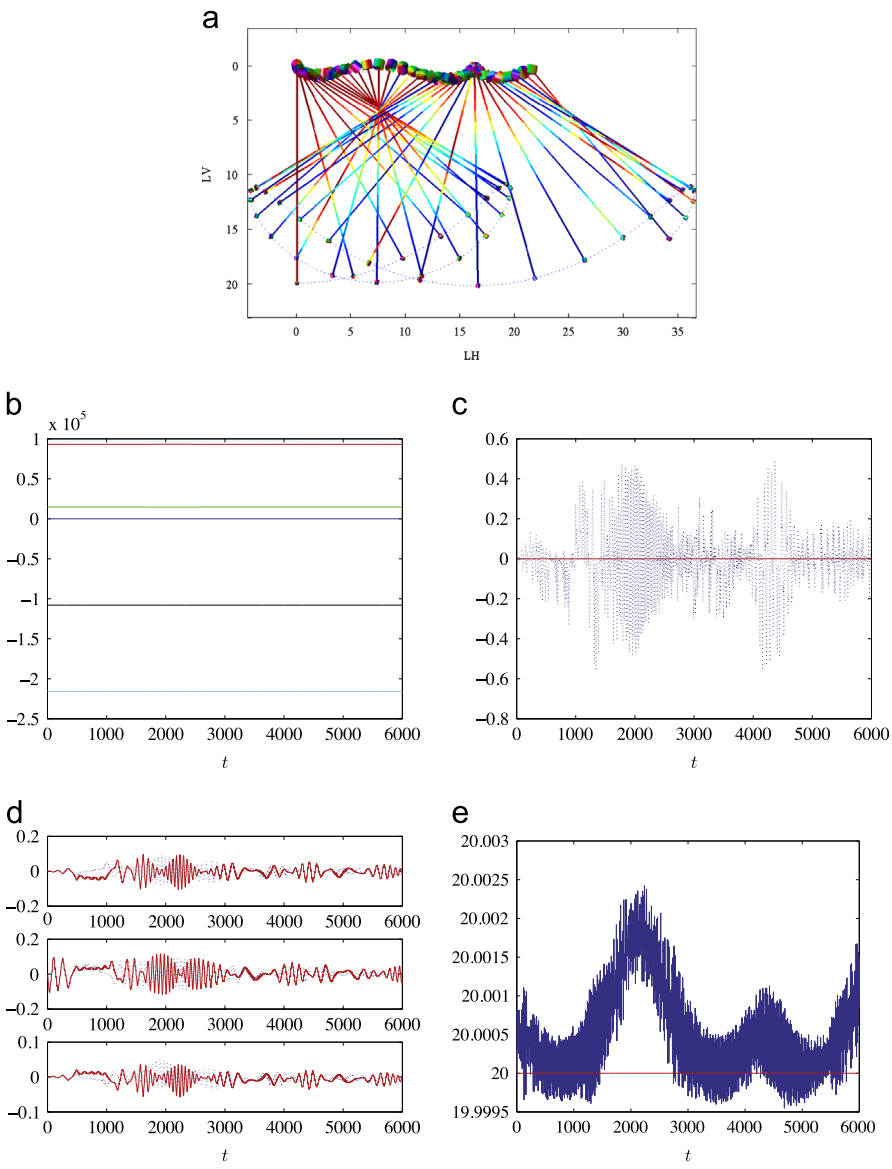

Fig. 3. Case 1: Circular orbit, Fixed unstretched tether length. (a) Snapshots observed in the LVLH frame (km) (The size of spacecraft is increased by a factor of 100 to illustrate the attitude dynamics.). (b) $T_{base}+T_{sub}$ (red), T_{tether} (green), $V_{gravity}$ (cyan), $V_{elastic}$ (blue), total energy (black) (10^6 J). (c) Computed total energy deviation $E(t)-E(0)$ (LGVI: red, RK: blue, dotted) (10^6 J). (d) Angular Velocity of the base spacecraft Ω (LGVI: red, RK: blue, dotted) (*rad*/*s*) (e) Unstretched length of the deployed part of the tether (red), stretched length (blue) (*km*). (For interpretation of the references to color in this figure caption, the reader is referred to the web version of this paper.)

the size of the spacecraft is increased by a factor of 100, and the relative strain distribution of the tether at each instant is represented by a color shading. (Animation that visualizes each maneuver of tethered spacecraft has also been submitted as supplementary materials.) The remaining subfigures show (b) the energy transfer, (c) the computed total energy deviation from its initial value, (d) the angular velocity of the base spacecraft, and (e) the unstretched/stretched length of the tether. For the first case and the third case, the computed total energy deviation and the angular velocity of the base spacecraft are compared with the results from the Runge–Kutta method.

In the first case, we observe a pendulum-like motion where the tether is taut and its stretched length is almost close to the unstretched length. But, one observes a strain wave that propagates along the tether, and nontrivial attitude dynamics for the base spacecraft and the sub-spacecraft. The proposed Lie group variational integrator exhibits excellent conservation properties, as shown in Table 1. The Runge–Kutta method exhibits relative large deviations in the total energy, and large errors in the preservation of the orthogonal structure of rotation matrices. As illustrated in Fig. 3(d), the errors in preserving the conserved quantities also cause errors in computing the angular velocities: there is a noticeable difference after $t=300$ s.

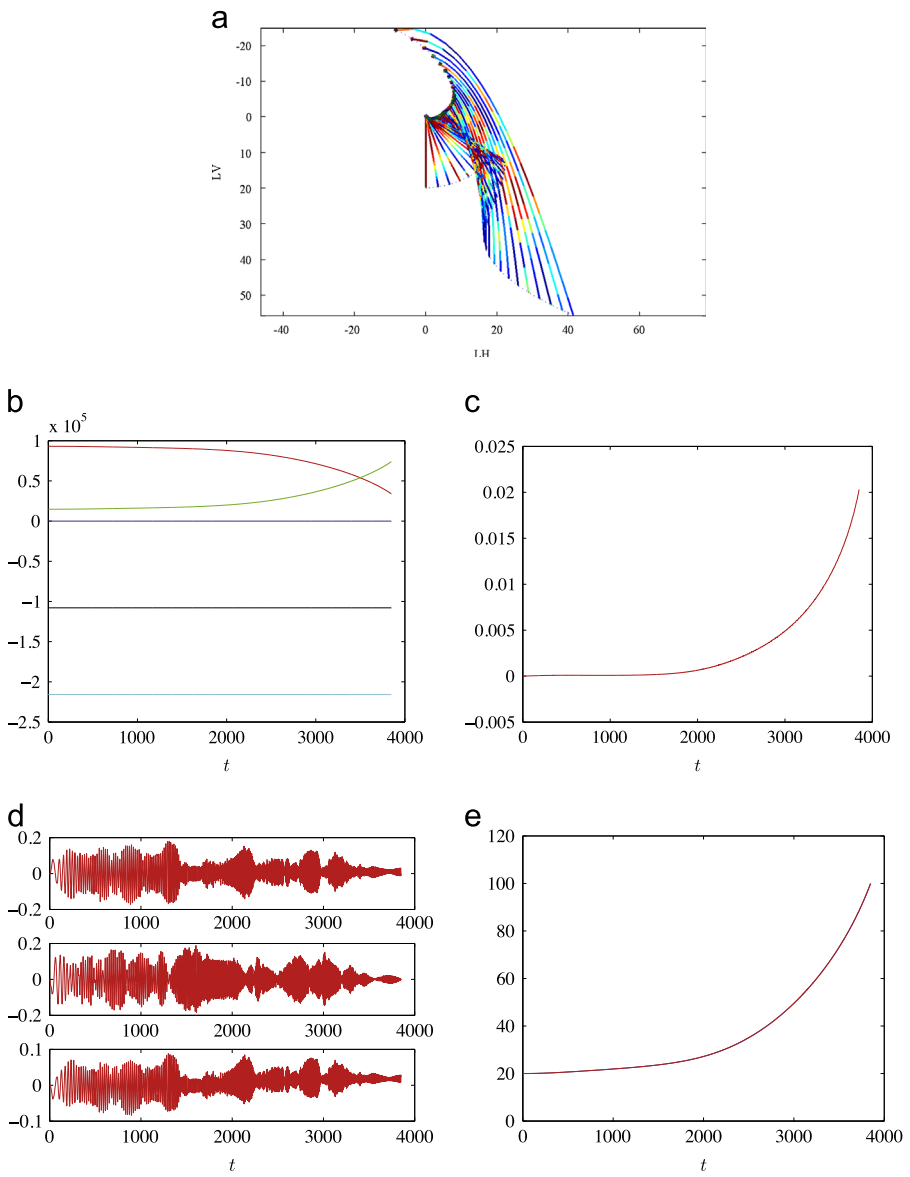

Fig. 4. Case 2: circular orbit, releasing tether. (a) Snapshots observed in the LVLH frame (km). (b) $T_{base}+T_{sub}$ (red), T_{tether} (green), $V_{gravity}$ (cyan), $V_{elastic}$ (blue), total energy (black) (10^6 J). (c) Computed total energy deviation $E(t)-E(0)$ (10^6 J). (d) Angular velocity of the base spacecraft Ω (rad/s). (e) Unstretched length of the deployed part of the tether (red), stretched length (blue) (km). (For interpretation of the references to color in this figure caption, the reader is referred to the web version of this paper.)

In the second case, the tether is deployed by gravity gradient effects between the base spacecraft and the sub-spacecraft. Due to the Carnot energy term discussed in the previous section, the total energy increases slightly. As the mass in the base spacecraft is transferred to the deployed portion of the tether, there is kinetic energy transfer from the base spacecraft into the deployed portion of tether, as seen in Fig. 4(b).

The third case is most challenging: there are in-plane and out-of-plane tumbling motions; the tether is stretched by 25%; the attitude dynamics of the spacecrafts are nontrivially excited with large angular velocities. As the altitude of tethered spacecraft increases, the kinetic energy is transferred to the gravitation potential energy, and there is also kinetic energy exchange between spacecraft and tether at a higher frequency. The proposed Lie group variational integrator computes the complex dynamics of this tethered spacecraft accurately, and it exhibits excellent conservation properties compared with Runge–Kutta method, as shown in Table 1.

One of the most distinct features of the proposed computational model of tethered spacecraft is that it explicitly takes account of the coupling between several dynamic modes, which have been ignored in most of the existing approaches. As a concrete example to demonstrate the coupling effect between the rotational dynamics of tethered spacecraft with the translational orbital dynamics, the third case is repeated while assuming that

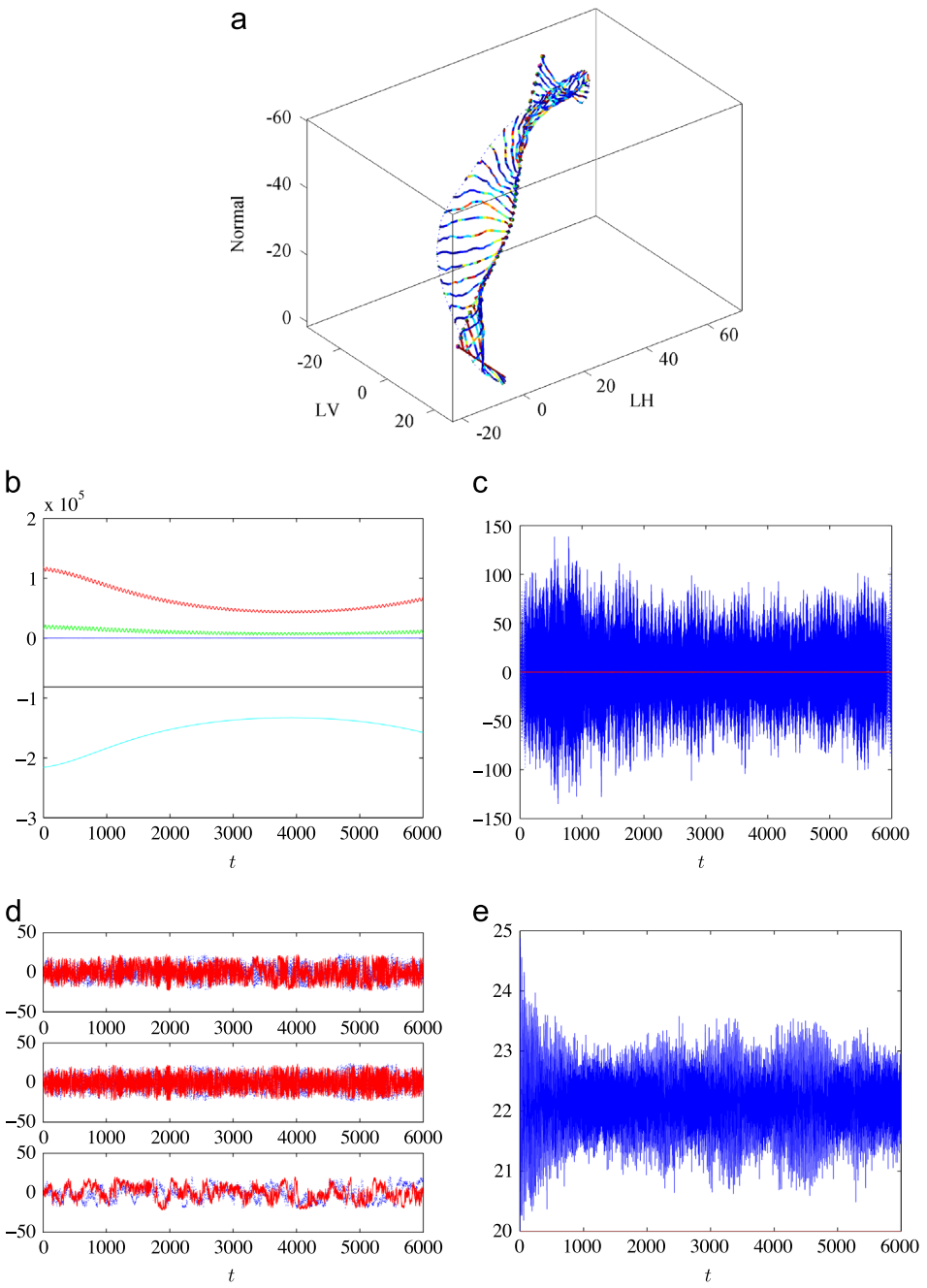

Fig. 5. Case 3: perturbed circular orbit, fixed unstretched tether length. (a) Snapshots observed in the LVLH frame for $t \leq 60$ s (km). (b) $T_{base}+T_{sub}$ (red), T_{tether} (green), $V_{gravity}$ (cyan), $V_{elastic}$ (blue), total energy (black) (10^6 J). (c) Computed total energy deviation $E(t)-E(0)$ (LGVI: red, RK: blue, dotted) (10^6 J). (d) Angular velocity of the base spacecraft Ω (LGVI: red, RK: blue, dotted) (rad/s). (e) Unstretched length of the deployed part of the tether (red), stretched length (blue) (km). (For interpretation of the references to color in this figure caption, the reader is referred to the web version of this paper.)

the base spacecraft and the sub-spacecraft are modeled as point masses, i.e., $\rho = \rho_s = 0$. The differences in the position of the base spacecraft and the sub-spacecraft between the full dynamics model proposed in this paper and the simplified model without the attitude dynamics are illustrated at Fig. 6(a) and (b). Ignoring the attitude dynamics causes mean errors of 1.03 km and 8.29 km in the computed position of the base spacecraft and the sub-spacecraft, respectively. This is a noticeable discrepancy considering the fact that the simulation period is slightly longer than one orbital period, and that the ratio of the rotational kinetic energy to the total kinetic energy is at the level of 10^{-5}. In particular, as illustrated at Fig. 6(c), the relative position of the sub-spacecraft with respect to the base spacecraft and the configuration of the tether could be drastically different. These illustrate the importance of the

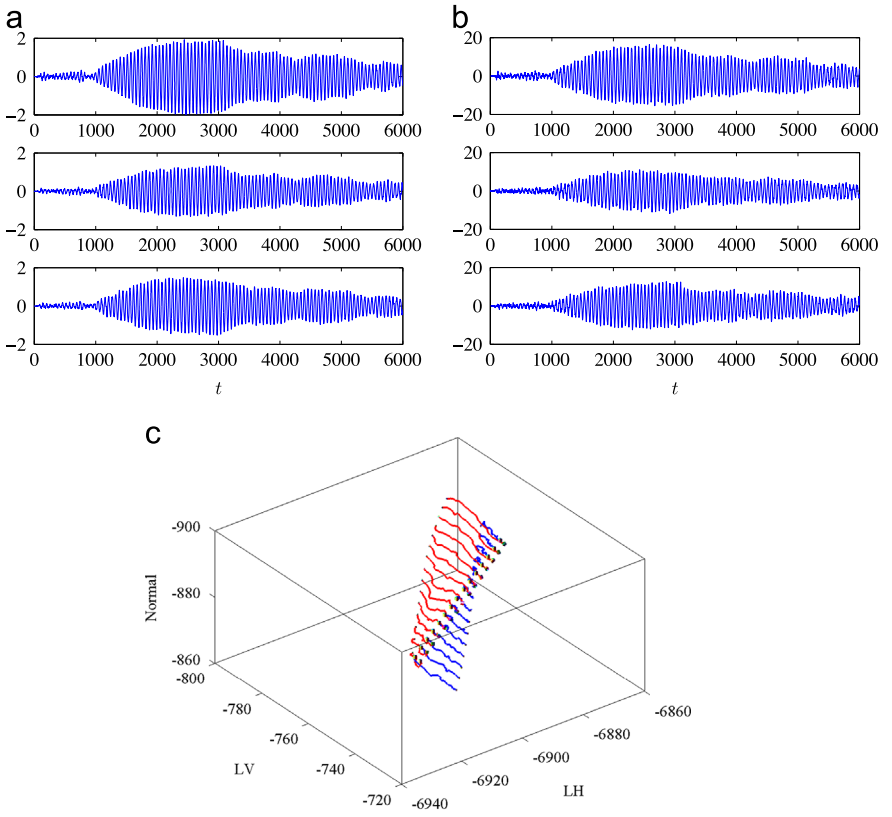

Fig. 6. Case 3: comparison with a simplified dynamic model where the attitude dynamics is ignored. (a) Difference in the position x of the base spacecraft (km). (b) Difference in the position $r_{N+1}+R_s\rho_s$ of the sub-spacecraft (km). (c) Snapshots observed in the LVLH frame (red: with attitude dynamics, blue: without attitude dynamics) (km, $2600 \le t \le 2610$). (For interpretation of the references to color in this figure caption, the reader is referred to the web version of this paper.)

nonlinear coupling effects between the attitude dynamics and the translational dynamics of tethered spacecraft in complex maneuvers.

6. Conclusions

We develop continuous-time equations of motion and a geometric numerical integrator for a tethered spacecraft model that includes tether deformation, spacecraft attitude dynamics, and a reeling mechanism. This provides an analytical model that is defined globally on the Lie group configuration manifold, and the Lie group variational integrator preserves the underlying geometric features, thereby yielding a reliable numerical simulation tool for complex maneuvers over a long time period. We also show that both continuous-time model and numerical integrators for tethered spacecraft can be derived using a variational framework.

The numerical results suggest that any small disturbance to the tethered spacecraft is propagated along the tether at a high velocity, which is determined by the material properties of tether. Since the points of contact between tether and spacecraft are displaced from the center of mass of the spacecraft, the elastic disturbances of the tether excite the rotational dynamics of spacecraft significantly. Therefore, it is critical to accurately model the reel mechanism, deformation of the tether, spacecraft rotational dynamics, and their interaction for obtaining realistic numerical predictions about how tethered spacecraft behave when performing aggressive maneuvers.

Future research directions include designing optimal orbital maneuvers of tethered spacecraft by adopting computational geometric optimization techniques based on the proposed Lie group variational integrator [28]. The presented tethered spacecraft model can be used for vibration analysis that includes the rotational dynamics of both spacecraft and a reel mechanism [9–11]. Also, it can be generalized for an arbitrary number of rigid bodies connected by multiple tethers [29,30]. The presence of multiple-timescales in the fully coupled system also naturally leads to the question of developing multiscale variational integrators.

Acknowledgments

This research has been supported in part by NSF under the Grants CMMI-1029445, 1243000, 1334759, 1335008, CNS-1337722, and DMS-1010687, 1065972.

Appendix A. Derivation of the Lie group variational integrator for a tethered spacecraft

A.1. Derivatives of the discrete Lagrangian

The Lie group variational integrator given by (37) is expressed in terms of the derivatives of the discrete Lagrangian and their co-tangent lift. Here, we describe how to compute the co-tangent lift and the co-Adjoint operator on the configuration manifold $\mathsf{G}=\mathbb{R}^3\times \mathrm{SO}(3)\times \mathbb{R}\times(\mathbb{R}^3)^{N+1}\times \mathrm{SO}(3)$ without introducing the formal definition of those operators.

The co-tangent lift of the left translation on a real space is the identity map on that real space. Using the product structure of the configuration manifold $\mathsf{G}=\mathbb{R}^3\times \mathrm{SO}(3)\times\mathbb{R}\times(\mathbb{R}^3)^{N+1}\times \mathrm{SO}(3)$, the derivative of the discrete Lagrangian with respect to $f_k=(\Delta x_k; F_k; \Delta s_{p_k}; \Delta r_{k,1},\ldots,\Delta r_{k,N+1}; F_{s_k})\in \mathsf{G}$ is given by

$$\mathsf{T}_e^*\mathsf{L}_{f_k}\cdot\mathbf{D}_{f_k}L_{d_k}=[\mathbf{D}_{\Delta x_k}L_{d_k};\ \mathsf{T}_I^*\mathsf{L}_{F_k}\cdot\mathbf{D}_{F_k}L_{d_k};\ \mathbf{D}_{\Delta s_{p_k}}L_{d_k};\ \mathbf{D}_{\Delta r_{1,k}}L_{d_k},\ldots,\mathbf{D}_{\Delta r_{N+1,k}}L_{d_k};\ \mathsf{T}_I^*\mathsf{L}_{F_{s_k}}\cdot\mathbf{D}_{F_{s_k}}L_{d_k}]. \tag{A.1}$$

Deriving the derivatives of the discrete Lagrangian with respect to Δx_k, Δs_{p_k} or $\Delta r_{k,a}$ is relatively straightforward. For example, from (31), (34), and (36), the derivatives of the discrete Lagrangian with respect to $x_k, \Delta x_k$ are given by

$$\mathbf{D}_{\Delta x_k}L_{d_k}=\frac{1}{h}(m+m_r+\bar{\mu}s_{p_k})\Delta x_k-\frac{h}{2}\mathbf{D}_{x_{k+1}}V_{k+1}, \tag{A.2}$$

$$\mathbf{D}_{x_k}L_{d_k}=-\frac{h}{2}\mathbf{D}_{x_k}V_k-\frac{h}{2}\mathbf{D}_{x_{k+1}}V_{k+1}, \tag{A.3}$$

where

$$\mathbf{D}_{x_k}V_k=GM(m+m_r+\bar{\mu}s_{p_k})\frac{x_k}{\|x_k\|^3}.$$

Similarly, from (32), the derivative of the discrete Lagrangian with respect to $\Delta r_{k,a}$ for $a=2,\ldots,N$ is given by

$$\begin{aligned}\mathbf{D}_{\Delta r_{k,a}}L_{d_k}&=h(\mathbf{D}_{\Delta r_{k,a}}T_{k,a-1}+\mathbf{D}_{\Delta r_{k,a}}T_{k,a})-\frac{h}{2}\mathbf{D}_{\Delta r_{k,a}}V_{k+1}\\&=\frac{1}{h}M_k^{12}\Delta r_{k,a-1}+\frac{2}{h}M_k^1\Delta r_{k,a}+\frac{1}{h}M_k^{12}\Delta r_{k,a+1}\\&\quad+\frac{1}{h}\left(M_{k,a}^{31}+M_{k,a-1}^{23}\right)\Delta s_{p_k}-\frac{h}{2}\mathbf{D}_{r_{k+1,a}}V_{k+1},\end{aligned} \tag{A.4}$$

where the derivative of the potential energy is given by

$$\begin{aligned}\mathbf{D}_{r_{k,a}}V_k&=2GM\bar{\mu}l_k\frac{r_{k,a-1}+r_{k,a}}{\|r_{k,a-1}+r_{k,a}\|^3}+2GM\bar{\mu}l_k\frac{r_{k,a}+r_{k,a+1}}{\|r_{k,a}+r_{k,a+1}\|^3}\\&\quad+\nabla V_{k,a-1}^e-\nabla V_{k,a}^e,\end{aligned} \tag{A.5}$$

$$\nabla V_{k,a}^e=\frac{EA}{l_k}\frac{\|r_{k,a+1}-r_{k,a}\|-l_k}{\|r_{k,a+1}-r_{k,a}\|}(r_{k,a+1}-r_{k,a}). \tag{A.6}$$

Expressions for the other derivatives of the discrete Lagrangian with respect to s_{p_k}, Δs_{p_k}, r_{k_1}, Δr_{k_1}, $r_{k,N+1}$, $\Delta r_{k,N+1}$ can be developed similarly.

Now we find the derivative of the discrete Lagrangian with respect to F_k. From (31), (35), and (36), we have

$$\mathbf{D}_{F_k}L_{d_k}\cdot\delta F_k=\frac{1}{h}\,\mathrm{tr}\left[-\delta F_k J_d\right].$$

Similar to (12), the variation of the rotation matrix F_k can be written as $\delta F_k=F_k\hat{\zeta}$ for a vector $\zeta\in\mathbb{R}^3$. From the definition of the co-tangent lift of the left translation, we have

$$(\mathsf{T}_I^*\mathsf{L}_{F_k}\cdot\mathbf{D}_{F_k}L_{d_k})\cdot\zeta=\frac{1}{h}\,\mathrm{tr}\left[-F_k\hat{\zeta}_k J_d\right].$$

By repeatedly applying the following property of the trace operator, $\mathrm{tr}[AB]=\mathrm{tr}[BA]=\mathrm{tr}[A^TB^T]$ for any $A,B\in\mathbb{R}^{3\times3}$, this can be written as $\mathrm{tr}\left[-F_k\hat{\zeta}_kJ_d\right]=\mathrm{tr}\left[-\hat{\zeta}_kJ_dF_k\right]=\mathrm{tr}\left[\hat{\zeta}_k\ F_k^TJ_d\right]=-\frac{1}{2}\,\mathrm{tr}\left[\hat{\zeta}_k\left(J_dF_k-F_k^TJ_d\right)\right]$. Using the property of the hat map, $x^Ty=-\frac{1}{2}\,\mathrm{tr}[\hat{x}\hat{y}]$ for any $x,y\in\mathbb{R}^3$, this can be further written as

$$\mathsf{T}_I^*\mathsf{L}_{F_k}\cdot\mathbf{D}_{F_k}L_{d_k}=\frac{1}{h}(J_dF_k-F_k^TJ_d)^\vee. \tag{A.7}$$

Similarly, we obtain

$$\begin{aligned}&\mathsf{T}_I^*\mathsf{L}_{F_{s_k}}\cdot\mathbf{D}_{F_{s_k}}L_{d_k}\\&\quad=\frac{1}{h}(J_{s_d}F_{s_k}-F_{s_k}^TJ_{s_d})^\vee+\frac{m_s}{h}\hat{\rho}_sF_{s_k}^TR_{s_k}^T\Delta r_{k,N+1}\\&\qquad-\frac{h}{2}GMm_s\hat{\rho}_sF_{s_k}^TR_{s_k}^T\frac{r_{k+1,N+1}+R_{s_{k+1}}\rho_s}{\|r_{k+1,N+1}+R_{s_{k+1}}\rho_s\|^3}.\end{aligned} \tag{A.8}$$

Expression for the derivatives of the discrete Lagrangian with respect to R_k and R_{s_k} are similarly developed.

The Lie group variational integrator given by (37) also involves the co-Adjoint map [19]. Using the product structure of the configuration manifold, the second term of (37), namely $\mathrm{Ad}^*_{f_k^{-1}}(\mathsf{T}_e^*\mathsf{L}_{f_k}\cdot\mathbf{D}_{f_k}L_{d_k})$, corresponds to the collection of the co-Adjoint maps for each element of $\mathsf{T}_e^*\mathsf{L}_{f_k}\cdot\mathbf{D}_{f_k}L_{d_k}$ given by (A.1).

The co-Adjoint map on a real space is the identity map on that real space. For example,

$$\mathrm{Ad}^*_{-\Delta x_k}(\mathbf{D}_{\Delta_k}L_{d_k})=\mathbf{D}_{\Delta_k}L_{d_k}. \tag{A.9}$$

The co-Adjoint map on SO(3) is given by $\mathrm{Ad}^*_{F_k^{-1}}p=F_kpF_k^T=(F_k\hat{p}F_k^T)^\vee$ for any $p\in(\mathbb{R}^3)^*\simeq\mathfrak{so}(3)^*$ to obtain

$$\mathrm{Ad}^*_{F_k^T}(\mathsf{T}_I^*\mathsf{L}_{F_k}\cdot\mathbf{D}_{F_k}L_{d_k})=\frac{1}{h}(F_kJ_d-J_dF_k)^\vee, \tag{A.10}$$

$$\begin{aligned}&\mathrm{Ad}^*_{F_{s_k}^T}\left(\mathsf{T}_I^*\mathsf{L}_{F_{s_k}}\cdot\mathbf{D}_{F_{s_k}}L_{d_k}\right)\\&\quad=\frac{1}{h}(F_{s_k}J_{s_d}-J_{s_d}F_{s_k}^T)^\vee+\frac{m_s}{h}F_{s_k}\hat{\rho}_sF_{s_k}^TR_{s_k}^T\Delta r_{k,N+1}\\&\qquad-\frac{h}{2}GMm_sF_{s_k}\hat{\rho}_sF_{s_k}^TR_{s_k}^T\frac{r_{k+1,N+1}+R_{s_{k+1}}\rho_s}{\|r_{k+1,N+1}+R_{s_{k+1}}\rho_s\|^3}.\end{aligned} \tag{A.11}$$

$$\begin{aligned}&\frac{1}{h}(m+m_r+\bar{\mu}s_{p_k})\Delta x_k+\frac{1}{h}M_k^1\Delta r_{k,1}+\frac{1}{h}M_k^{12}\Delta r_{k,2}+\frac{1}{h}M_{k,1}^{31}\Delta s_{p_k}\\&\quad=\frac{1}{h}(m+m_r+\bar{\mu}s_{p_{k-1}})\Delta x_{k-1}+\frac{1}{h}M_{k-1}^1\Delta r_{k-1,1}\\&\qquad+\frac{1}{h}M_{k-1}^{12}\Delta r_{k-1,2}+\frac{1}{h}M_{k-1,1}^{31}\Delta s_{p_{k-1}}\\&\qquad+\frac{\mu}{6Nh}(3N-2)\Delta s_{p_k}\Delta r_{k,2}+\frac{\mu}{6Nh}(3N-1)\Delta s_{p_k}\Delta r_{k,1}\\&\qquad-h\mathbf{D}_{x_k}V_k-h\mathbf{D}_{r_{k,1}}V_k,\end{aligned} \tag{A.12}$$

$$x_k+\Delta x_k+R_kF_k\rho=r_{k,1}+\Delta r_{k,1}, \tag{A.13}$$

$$\begin{aligned}&\frac{1}{h}M_k^0\Delta s_{p_k}+\frac{1}{h}M_{k,1}^{31}\Delta r_{k,1}+\frac{1}{h}\sum_{a=2}^{N}\left(M_{k,a}^{31}+M_{k,a-1}^{23}\right)\Delta r_{k,a}\\&\quad+\frac{1}{h}M_{k,N}^{23}\Delta r_{k,N+1}\end{aligned}$$

$$= \frac{1}{h}M_{k-1}^{0}\Delta s_{p_{k-1}} + \frac{1}{h}M_{k-1,1}^{31}\Delta r_{k-1,1} + \frac{1}{h}\sum_{a=2}^{N}(M_{k-1,a}^{31} + M_{k-1,a-1}^{23})\Delta r_{k-1,a} + \frac{1}{h}M_{k-1,N}^{23}\Delta r_{k-1,N+1} + \frac{1}{2h}\overline{\mu}\Delta x_k\cdot\Delta x_k + \frac{1}{3h}\overline{\mu}\Delta s_{p_k}^2 - \frac{\mu}{6Nh}\sum_{a=1}^{N}\left(\Delta r_{k,a}\cdot\Delta r_{k,a} + \Delta r_{k,a+1}\cdot\Delta r_{k,a+1} + \Delta r_{k,a}\cdot\Delta r_{k,a+1}\right) - h\mathbf{D}_{s_{p_k}}V_k + h\frac{u_k}{d} - \frac{h}{2l_k^2}\left(\overline{\mu}\Delta s_{p_k}^2/h^2 + EA\right)(\|r_{k,2}-r_{k,1}\|-l_k)^2, \tag{A.14}$$

$$\frac{1}{h}M_k^{12}\Delta r_{k,a-1} + \frac{2}{h}M_k^{1}\Delta r_{k,a} + \frac{1}{h}M_k^{12}\Delta r_{k,a+1} + \frac{1}{h}\left(M_{k,a}^{31} + M_{k,a-1}^{23}\right)\Delta s_{p_k} = \frac{1}{h}M_{k-1}^{12}\Delta r_{k-1,a-1} + \frac{2}{h}M_{k-1}^{1}\Delta r_{k-1,a} + \frac{1}{h}M_{k-1}^{12}\Delta r_{k-1,a+1} + \frac{1}{h}(M_{k-1,a}^{31} + M_{k-1,a-1}^{23})\Delta s_{p_{k-1}} + \frac{\mu}{6Nh}(1+3N-3a)\Delta s_{p_k}\Delta r_{k,a+1} - \frac{\mu}{3Nh}\Delta s_{p_k}\Delta r_{k,a} - \frac{\mu}{6Nh}(5+3N-3a)\Delta s_{p_k}\Delta r_{k,a-1} - h\mathbf{D}_{r_{k,a}}V_k, \tag{A.15}$$

$$\frac{1}{h}\left(M_k^2 + m_s\right)\Delta r_{k,N+1} + \frac{1}{h}M_k^{12}\Delta r_{k,N} + \frac{1}{h}M_{k,N}^{23}\Delta s_{p_k} + \frac{1}{h}m_s R_{s_k}(F_{s_k} - I)\rho_s = \frac{1}{h}\left(M_{k-1}^2 + m_s\right)\Delta r_{k-1,N+1} + \frac{1}{h}M_{k-1}^{12}\Delta r_{k-1,N} + \frac{1}{h}M_{k-1,N}^{23}\Delta s_{p_{k-1}} + \frac{1}{h}m_s R_{s_k}(F_{s_{k-1}} - I)\rho_s - \frac{\mu}{6Nh}\Delta s_{p_k}\Delta r_{k,N+1} - \frac{\mu}{3Nh}\Delta s_{p_k}\Delta r_{k,N} - h\mathbf{D}_{r_{k,N+1}}V_k, \tag{A.16}$$

$$\frac{1}{h}(F_k J_d - J_d F_k^T)^{\vee} + \hat{\rho}R_k^T\left(\frac{1}{h}M_k^1\Delta r_{k,1} + \frac{1}{h}M_k^{12}\Delta r_{k,2} + \frac{1}{h}M_{k,1}^{31}\Delta s_{p_k}\right) = \frac{1}{h}(J_d F_{k-1} - F_{k-1}^T J_d)^{\vee} + \hat{\rho}R_k^T\left(\frac{1}{h}M_{k-1}^1\Delta r_{k-1,1} + \frac{1}{h}M_{k-1}^{12}\Delta r_{k-1,2} + \frac{1}{h}M_{k-1,1}^{31}\Delta s_{p_{k-1}}\right) + \hat{\rho}R_k^T\left(\frac{\mu}{6Nh}(3N-2)\Delta s_{p_k}\Delta r_{k,2} + \frac{\mu}{6Nh}(3N-1)\Delta s_{p_k}\Delta r_{k,1} - h\mathbf{D}_{r_{k,1}}V_k\right) - hu_k e_2, \tag{A.17}$$

$$\frac{1}{h}(F_{s_k}J_{s_d} - J_{s_d}F_{s_k}^T)^{\vee} = \frac{1}{h}(J_{s_d}F_{s_{k-1}} - F_{s_{k-1}}^T J_{s_d})^{\vee} - \frac{m_s}{h}\hat{\rho}_s R_{s_k}^T(\Delta r_{k,N+1} - \Delta r_{k-1,N+1}) - hGMm_s\hat{\rho}_s R_{s_k}^T\frac{r_{k,N+1} + R_{s_k}\rho_s}{\|r_{k,N+1} + R_{s_k}\rho_s\|^3}. \tag{A.18}$$

A.2. Lie group variational integrator

Once the derivatives of the discrete Lagrangian and their co-Adjoint maps are obtained, they are substituted into (37) and (38) with the contributions of the external control moment (39), and the Carnot energy loss term (40). The resulting discrete-time Euler–Lagrange equations of tethered spacecraft are given by (A.12)–(A.18), where the constraint on the continuity of the tether at the beginning of the guideway which is given by (A.13) and (A.15) is satisfied for $a=2,\ldots,N$.

For a given $g_k = (x_k; R_k; s_{p_k}; r_{k,1}, \ldots r_{k,N+1}; R_{s_k})$, we solve (A.12)–(A.15) for the relative update $f_k = (\Delta x_k; F_k; \Delta s_{p_k}; \Delta r_{k,1}, \ldots, \Delta r_{k,N+1}; F_{s_k})$. Then, the configuration at the next step, namely g_{k+1} is obtained by (30). This yields a discrete-time Lagrangian flow map $(g_k, f_k) \mapsto (g_{k+1}, f_{k+1})$, and this is iterated.

Special cases: If we set $\Delta s_{p_k} \equiv 0$ for all k, then the discrete-time Euler–Lagrange equations provide a geometric numerical integrator for tethered spacecraft with a fixed unstretched tether length. If we chose $\rho = \rho_c = 0$, then these equations describe the dynamics of two point masses connected by tether and a reeling mechanism.

Computational approach: These Lie group variational integrators for tethered spacecraft are implicit: at each time-step, we need to solve nonlinear implicit equations to find the relative update $f_k \in \mathsf{G}$. Therefore, it is important to develop an efficient computational approach for these implicit equations. This computational method should preserve the group structure of f_k, and in particular, the orthogonal structure of the rotation matrix $F_k \in \mathrm{SO}(3)$ should be preserved. The key idea of the computational approach proposed in this paper is to express the rotation matrix F_k in terms of a vector $c_k \in \mathbb{R}^3$ using the Cayley transformation [17]:

$$F_k = (I + \hat{c}_k)(I - \hat{c}_k)^{-1}. \tag{A.19}$$

Since the rotation matrix F_k represents the relative attitude update between two adjacent integration steps, it is a near-to-identity transformation when the time-step h is sufficiently small. As such, the expression above remains valid for numerical simulations even though the Cayley transformation is only a local diffeomorphism between $\mathbb{R}^3$ and $\mathrm{SO}(3)$ about $c_k = 0$ and $F_k = I$.

Our computational approach is as follows. The implicit equations for F_k and F_{s_k}, namely (A.17) and (A.18), are rewritten in terms of vectors c_k, c_{s_k} using (A.19). Then, the relative update map is expressed by a vector $X_k = [\Delta x_k; c_k; \Delta s_{p_k}; \Delta r_{k,1}, \ldots \Delta r_{k,N+1}; c_{s_k}] \in \mathbb{R}^{3(N+1)+10}$, which is solved by using a Newton iteration. After the vector X_k converges, the rotation matrices F_k and F_{s_k} are computed by (A.19), to obtain $f_k \in \mathsf{G}$.

This computational approach is desirable, since the implicit equations are solved numerically using operations in a linear vector space. Rotation matrices, F_k and F_{s_k}, are computed by numerical iterations on $\mathbb{R}^6$, and its orthogonal structure is automatically preserved by (A.19). It has been shown that this computational approach is numerically efficient [23].

Appendix B. Supplementary material

Supplementary data associated with this paper can be found in the online version of http://dx.doi.org/10.1016/j.actaastro.2014.02.021.

References

[1] M. Cosmo, E. Lorenzini, Tethers in Space Handbook, Technical Report, NASA Marshall Space Flight Center, 1997.

[2] E. Lorenzini, M. Grossi, M. Cosmo, Low altitude tethered mars probe, Acta Astronaut. 21 (1990) 1–12.
[3] L. Less, C. Bruno, C. Ullvieri, U. Ponzi, M. Parisse, G. Laneve, G. Vannaroni, M. Dobrowolny, F. De Venuto, B. Bertotti, L. Anselmo, Satellite de-orbiting by means of electrodynamic tethers, Part I: general concepts and requirements, Acta Astronaut. 50 (2002) 399–406.
[4] Young engineers' satellite 2, European Space Agency, URL: ⟨http://www.esa.int/SPECIALS/YES/index.html⟩.
[5] P. Williams, Simple approach to orbital control using spinning electrodynamic tethers, J. Spacecraft Rockets 43 (2006) 253–256.
[6] V. Beletsky, E. Levin, Dynamics of Space Tether Systems American Astronautical Society, Washington DC, 1993.
[7] L. Somenzi, L. less, J. Pelaez, Linear stability analysis of electrodynamic tethers, J. Guid. Control Dyn. 28 (2005) 843–849.
[8] G. Tyc, R. Han, Attitude dynamics investigation of the OEDIPUS-A tethered rocket payload, J. Spacecraft Rockets 32 (1995) 133–141.
[9] A. Misra, D. Xu, On vibrations of orbiting tethers, Acta Astronaut. 13 (1986) 587–597.
[10] S. Kalaycioglu, A. Misra, Approximate solutions for vibrations of deploying appendages, J. Guid. Control Dyn. 14 (1991) 287–293.
[11] F. Vigneron, A. Jablonski, R. Chandrashaker, J. Bergmans, B. McClure, G. Tyc, Comparison of analytical modeling of OEDIPUS tethers with data from tether laboratory, J. Guid. Control Dyn. 20 (1997) 471–478.
[12] W. Steiner, J. Zemann, A. Steindl, H. Troger, Numerical study of large amplitude oscillations of a two-satellite continuous tether system with a varying length, Acta Astronaut. 35 (1995) 607–621.
[13] M. Krupa, W. Poth, M. Schagerl, A. Steindl, W. Steiner, H. Troger, Modelling, dynamics and control of tethered satellites systems, Nonlinear Dyn. 43 (2006) 73–96.
[14] K. Mankala, S. Agrawal, Dynamic modeling and simulation of satellite tethered systems, ASME J. Vib. Acoust. 127 (2005) 144–156.
[15] T. Lee, M. Leok, N. McClamroch, Computational dynamics of a 3D elastic string pendulum attached to a rigid body and an inertially fixed reel mechanism, Nonlinear Dyn. 64 (2011) 97–115.
[16] T. Lee, M. Leok, N. McClamroch, Dynamics of a 3D elastic string pendulum, in: Proceedings of IEEE Conference on Decision and Control, 2009, pp. 3347–3352.
[17] E. Hairer, C. Lubich, G. Wanner, Geometric Numerical Integration. Springer Series in Computational Mechanics, vol. 31, Springer, New York, 2000.
[18] T. Lee, Computational geometric mechanics and control of rigid bodies (Ph.D. thesis), University of Michigan, 2008.
[19] J. Marsden, T. Ratiu, 2nd ed. Introduction to Mechanics and Symmetry of Texts in Applied Mathematics, vol. 17, Springer-Verlag, 1999.
[20] E. Crellin, F. Janssens, D. Poelaert, W. Steiner, H. Troger, On balance and variational formulations of the equations of motion of a body deploying along a cable, J. Appl. Mech. 64 (1997) 369–374.
[21] J. Marsden, M. West, Discrete mechanics and variational integrators, in: Acta Numerica, vol. 10, Cambridge University Press, Cambridge, UK, 2001, pp. 317–514.
[22] A. Iserles, H. Munthe-Kaas, S. Nørsett, A. Zanna, Lie-group methods, in: Acta Numerica, vol. 9, Cambridge University Press, Cambridge, UK, 2000, pp. 215–365.
[23] T. Lee, M. Leok, N.H. McClamroch, Lie group variational integrators for the full body problem in orbital mechanics, Celest. Mech. Dyn. Astron. 98 (2007) 121–144.
[24] B. Leimkuhler, S. Reich, Simulating Hamiltonian Dynamics, Cambridge Monographs on Applied and Computational Mathematics, vol. 14, Cambridge University Press, Cambridge, UK, 2004.
[25] N. Newmark, A method of computation for structural dynamics, ASCE J. Eng. Mech. 85 (1959) 67–94.
[26] T. Hughes, The Finite Element Method—Linear Static and Dynamic Finite Element Analysis, Prentice Hall, Upper Saddle River, NJ, 1987.
[27] D. Scheeres, E. Fahnestock, S. Ostro, J. Margot, L. Benner, S. Broschart, J. Bellerose, J. Giorgini, M. Nolan, C. Magri, P. Pravec, P. Scheirich, R. Rose, R. Jurgens, E.D. Jong, S. Suzuki, Dynamical configuration of binary near-Earth asteroid (66391) 1999 KW4, Science 314 (2006) 1280–1283.
[28] T. Lee, M. Leok, N.H. McClamroch, Computational geometric optimal control of rigid bodies, Commun. Inf. Syst. 8 (2008) 445–472. (Special issue dedicated to R.W. Brockett).
[29] A. Misra, V. Modi, Three-dimensional dynamics and control of tether-connected n-body systems, Acta Astronaut. 26 (1992) 77–84.
[30] A. Misra, G. Diamond, Dynamics of a subsatellite system supported by two tethers, J. Guid. Control Dyn. 9 (1986) 12–16.